Supplemental material to this article can be found at:
http://dmd.aspetjournals.org/content/suppl/2015/03/24/dmd.114.061713.DC1

1521-009X/43/6/803–811$25.00
Drug Metabolism and Disposition
http://dx.doi.org/10.1124/dmd.114.061713
Drug Metab Dispos 43:803–811, June 2015

Mechanistic Investigation of the Preclinical Pharmacokinetics and Interspecies Scaling of PF-05231023, a Fibroblast Growth Factor 21–Antibody Protein Conjugate

Craig Giragossian, Chandra Vage, Jun Li, Kathleen Pelletier, Nicole Piché-Nicholas, Manoj Rajadhyaksha, Jennifer Liras, Alison Logan, Roberto A. Calle, and Yan Weng

Pfizer Inc., Groton, Connecticut (C.G., C.V., Ju.L., K.P., M.R., A.L.); and Pfizer Inc., Cambridge, Massachusetts (N.-P.N., Je.L., R.A.C., Y.W.)

Received October 21, 2014; accepted March 16, 2015

ABSTRACT

PF-05231023, a long-acting fibroblast growth factor 21 (FGF21) analog, was generated by covalently conjugating two engineered [des-His1, Ala129Cys]FGF21 molecules to a nontargeting human $IgG_{1\kappa}$ scaffold. The pharmacokinetics (PK) of PF-05231023 after i.v. and s.c. administration was evaluated in rats and monkeys using two enzyme-linked immunosorbent assays with high specificity for biologically relevant intact N termini (NT) and C termini (CT) of FGF21. Intact CT of FGF21 displayed approximately 5-fold faster systemic plasma clearance (CL), an approximately 2-fold lower steady-state volume of distribution, and at least 5-fold lower bioavailability compared with NT. In vitro serum stability studies in monkeys and humans suggested that the principal CL mechanism for PF-05231023 was degradation by serum proteases. Direct scaling of in vitro serum degradation rates for intact CT of FGF21 underestimated in vivo CL 5-fold, 1.4-fold, and 2-fold in rats, monkeys, and humans, respectively. The reduced steady-state volume of distribution and the bioavailability for intact CT relative to NT in rats and monkeys were compatible with proteolytic degradation occurring outside the plasma compartment via an unidentified mechanism. Human CL and PK profiles for intact NT and CT of FGF21 were well predicted using monkey single-species allometric and Dedrick scaling. Physiologically based pharmacokinetic models incorporating serum stability data and an extravascular extraction term based on differential bioavailability of intact NT and CT of FGF21 in monkeys improved accuracy of human PK predictions relative to Dedrick scaling. Mechanistic physiologically based pharmacokinetic models of this nature may be highly valuable for predicting human PK of fusion proteins, synthetically conjugated proteins, and other complex biologics.

Introduction

Fibroblast growth factor 21 (FGF21) is a 19-kDa endocrine hormone that modulates lipid and glucose homeostasis (Belouski et al., 2010; Gimeno and Moller, 2014). The N terminus of FGF21 displays affinity for several fibroblast growth factor receptors (FGFRs), including FGFR1c, FGFR3c, and FGFR4, whereas the C terminus binds to the membrane-associated cofactor β-klotho. Truncation of N termini (NT) by six or more residues, or C termini (CT) by two or more residues, decreased in vitro potency more than 10-fold, suggesting that potent functional activity was derived from both termini of FGF21 (Micanovic et al., 2009; Yie et al., 2009). In diabetic animal models and patients with type 2 diabetes, recombinant fibroblast growth factor 21 (rFGF21) and its analogs demonstrated dose-dependent reductions in low-density lipoprotein cholesterol, apolipoproteins, fasting triglycerides, fasting insulin, and body weight, as well as dose-dependent elevations of high-density lipoprotein cholesterol and adiponectin (Adams et al., 2013; Gaich et al., 2013; Kharitonenkov et al., 2013; Smith et al., 2013). Although dose-dependent reductions in blood glucose have been observed in diabetic rodent and nonhuman primate models, thus far only a trend toward lower fasting blood glucose has been observed in human clinical studies (Gaich et al., 2013). Although the precise mechanism by which FGF21 exerts its pharmacological actions has not been deduced, both NT and CT are believed to be important for potent regulation of these processes.

The highly desirable pharmacology profile of FGF21 has generated significant interest as a potential therapy for type 2 diabetes and/or dyslipidemia; however, the full therapeutic potential of FGF21 may be limited by its short in vivo persistence. Systemic plasma clearance (CL) of rFGF21 in mice and monkeys was comparable to the glomerular filtration rate in each respective species, resulting in half-lives on the order of 0.5 to 2 hours (Kharitonenkov et al., 2007). Furthermore, CL of NT and CT immunoreactivity was indistinguishable in mice, suggesting that passive renal filtration was the primary CL mechanism for rFGF21 (Hager et al., 2013). Consistent with this hypothesis, endogenous levels of FGF21 were elevated more than 15-fold in patients with impaired renal function compared with controls (Stein et al., 2009).

At the time of data generation, all authors were employees and stockholders of Pfizer Inc. Pfizer Inc. provided support in the form of salaries for the authors but did not have any additional role in the study design, data collection and analysis, decision to publish, or preparation of the manuscript.

dx.doi.org/10.1124/dmd.114.061713.

This article has supplemental material available at dmd.aspetjournals.org.

ABBREVIATIONS: ADA, anti-drug antibody; CL, systemic plasma clearance; CT, C termini; FGF21, fibroblast growth factor 21; FGFR, fibroblast growth factor receptor; HRP, horseradish peroxidase; mAb, monoclonal antibody; NT, N termini; PBPK, physiologically based pharmacokinetics; PF-05231023, [des-His1, Ala129Cys]FGF21-human IgG1 conjugate; PK, pharmacokinetics; rFGF21, recombinant fibroblast growth factor 21; $t_{1/2}$, elimination half-life; V_{ss}, steady-state volume of distribution.

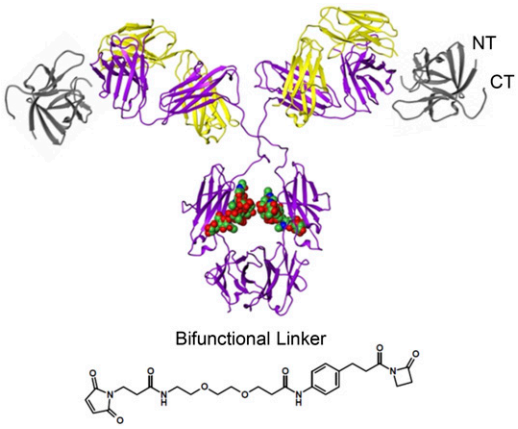

Fig. 1. Ribbon representation of the structure of PF-05231023. Light and heavy chains of the $IgG_{1\kappa}$ scaffold are depicted in yellow and purple, respectively. FGF21 is depicted in gray.

A variety of modalities have been utilized to extend the half-life of rFGF21, including pegylation, Fc fusion, and antibody conjugation (Reitman, 2013). Site-specific conjugation of 30-kDa polyethylene glycol to FGF21 demonstrated 10- to 50-fold improvements in CL/F compared with rFGF21, albeit at the expense of 5- to 10-fold reductions in in vitro potency (Mu et al., 2012). Fusion of NT (Fc-FGF21) or CT of FGF21 (FGF21-Fc) to the Fc fragment of $hIgG_1$ right-shifted in vitro potency 2- to 4-fold and 1000-fold, respectively (Hecht et al., 2012). The slightly reduced in vitro potency of Fc-FGF21 was offset by a 30-fold increase in serum persistence. However, reducing passive renal filtration of FGF21 by increasing its molecular weight had the untoward consequence of uncovering latent proteolytic cleavage sites in NT and CT of FGF21, resulting in only modest enhancements in monkey CL compared with marketed Fc-fusion proteins and therapeutic monoclonal antibodies (mAbs) (7.96 ml/h per kg versus 0.2–0.6 ml/h per kg). Stabilization of the C-terminal cleavage site through site-directed mutagenesis (Ser171Pro) decreased CL of intact Fc-FGF21 an additional 5-fold (Hager et al., 2013). As an alternative to Fc-fusion proteins, which require N-terminal or C-terminal coupling of FGF21 to the Fc domain, direct chemical conjugation of FGF21 to an antibody scaffold via a bifunctional synthetic linker enabled site-specific conjugation, thereby maximizing both potency and serum persistence. Engineered site-specific linkage sites remote from the NT and CT of FGF21 preserved in vitro potency while increasing serum persistence of FGF21 30- to 90-fold (Huang et al., 2013).

PF-05231023 (CVX-343), a long-acting FGF21 analog, consists of two molecules of [des-His1, Ala129Cys]FGF21 covalently linked to a humanized $IgG_{1\kappa}$ mAb backbone via a maleimide-azetidinone linker (Fig. 1) (Huang et al., 2013). PF-05231023 demonstrated comparable in vitro potency, enhanced pharmacokinetics (PK), and prolonged in vivo pharmacodynamics relative to rFGF21. The PK of PF-05231023 in rodents and nonhuman primates was previously characterized using a sandwich enzyme-linked immunosorbent assay with specificity for the mid-region of FGF21 (Huang et al., 2013). However, this assay lacked specificity for measuring the bioactive NT and CT of FGF21. In this study, immunoassays with high specificity for intact NT and CT of FGF21 were used to characterize the PK of PF-05231023 after i.v. and s.c. administration. In vitro serum stability studies were used to investigate the CL mechanism for PF-05231023 and to enable human PK predictions. A variety of scaling methodologies, including direct scaling of in vitro serum degradation rates, single-species allometric scaling, Dedrick scaling, and physiologically based pharmacokinetics (PBPK) modeling that incorporated serum stability and extravascular degradation terms were used to predict CL and PK profiles of PF-05231023 in humans.

Materials and Methods

Reagents. PF-05231023 was produced by the Pfizer Biotherapeutics Center of Excellence (St. Louis, MO). Mouse anti-$IgG_{1\kappa}$ idiotypic antibody and mouse anti-FGF21 C-terminal and N-terminal antibodies were generated by Pfizer.

Bioanalytical Assays. Four enzyme-linked immunosorbent assays were used to measure NT of FGF21, CT of FGF21, total FGF21, and total IgG, respectively. Mouse anti-FGF21 mAbs recognizing NT and CT were generated using peptide immunogens H2N-PIPDSSPLLQFGGC-OH and H2N-CGGPSQGRSPSYAS-OH, respectively. Antibodies displayed high specificity for the first and last two residues of the NT and CT of [des-His1]rFGF21, respectively. NT and CT of FGF21 were measured using an anti-idiotype capture reagent that recognized the mAb scaffold of PF-05231023, biotin-labeled anti–N-terminal or anti–C-terminal secondary antibodies, and streptavidin horseradish peroxidase (HRP). Total FGF21 was measured using an anti-FGF21 antibody that did not recognize the first 6 N-terminal amino acids or the last 32 C-terminal amino acids of rFGF21, designated as anti–mid-region FGF21. In the total FGF21 assay, PF-05231023 was captured with the anti–mid-region FGF21 mAb and was detected with an anti–hIgG-HRP–labeled antibody (Huang et al., 2013). Total IgG was measured

TABLE 1

Summary of key PK parameters of PF-05231023 after a single i.v. dose in rats and monkeys

The C_{max} and area under the curve were dosed normalized to 1 mg/kg. Rat PK parameters for total IgG were estimated using population modeling of composite steady-state concentrations upon repeat dose administration. ADAs (1%–10% incidence) did not appear to affect the PK of total IgG in rats.

Species/PK Assays	CL	V_c	V_{ss}	$t_{1/2}$	C_{max}/Dose	AUC_{0-t}/Dose	$AUC_{0-\infty}$/Dose
	ml/h per kg	*ml/kg*	*ml/kg*	*h*	*μg/ml*	*μg·h/ml*	*μg·h/ml*
Rats							
Intact CT	11.7 ± 0.33	29.6 ± 2.45	38.0 ± 2.90	6.30 ± 0.085	30.4 ± 2.57	85.5 ± 2.30	85.7 ± 2.30
Intact NT	3.59 ± 0.373	35.5 ± 13.6	70.9 ± 16.9	22.7 ± 2.16	30.3 ± 1.01	280 ± 26.6	281 ± 26.4
Total FGF21	2.11	51.9	111	97.3	18.5	466	474
Total IgG	1.29	30.2	199	286	20.5	699	775
Monkeys							
Intact CT	12.1 ± 4.19	41.3 ± 4.18	37.8 ± 3.17	3.02 ± 1.36	22.2 ± 1.99	88.4 ± 27.3	89.7 ± 28.0
Intact NT	2.61 ± 0.421	41.5 ± 4.52	103 ± 7.39	59.8 ± 8.53	23.4 ± 1.91	386 ± 57.6	391 ± 58.0
Total FGF21	2.34	38.1	102	82.0	25.7	427	429
Total IgG	1.48	37.0	230	209	26.2	620	678

$AUC_{0-\infty}$, area under concentration-time curve from 0 to infinity; AUC_{0-t}, area under concentration-time curve from 0 to the last measured time point; V_c, central distribution volume.

TABLE 2

Summary of key PK parameters for intact NT and CT in rats and monkeys after a single s.c. dose

Species	Dose	$t_{1/2}$	T_{max}	C_{max}	AUC_{0-t}	$AUC_{0-\infty}$	F%
	mg/kg	*h*	*h*	*μg/ml*	*μg·h/ml*	*μg·h/ml*	
Rats							
Intact CT	10	N.D.	N.D.	N.D.	N.D.	N.D.	N.D.
Intact NT	10	20.7 ± 6.07	30 ± 12	36.6 ± 14.9	1920 ± 794	1920 ± 794	68.3
Monkeys							
Intact CT	1	N.C.	4.0 ± 2.3	1.32 ± 0.568	9.11 ± 4.63	N.C.	10.2
Intact NT	1	56.8 ± 6.88	6.0 ± 0.0	3.08 ± 1.02	222 ± 54.5	228 ± 53.7	58.3

$AUC_{0-\infty}$, area under concentration-time curve from 0 to infinity; AUC_{0-t}, area under concentration-time curve from 0 to last measured time point; F%, bioavailability; N.C., not calculated due to insufficient data points; N.D., not determined because all concentrations were below limit of detection limit.

using a polyclonal anti-human IgG capture reagent and detected with an HRP-labeled polyclonal anti-human IgG reagent.

Pharmacokinetic Studies. All animal studies were conducted in accordance with animal care and use protocols approved by the Institutional Animal Care and Use Committee of Pfizer Inc. Single-dose PK of N-terminal and C-terminal FGF21 immunoreactivity of PF-05231023 was assessed in Wistar Hannover rats and cynomolgus monkeys. Male rats (n = 4/route) weighing approximately 250 g received a single 10 mg/kg i.v. dose in the tail vein or a s.c. dose between the shoulders. Male monkeys (n = 4/route) weighing 3 to 4 kg received either a single 1 mg/kg i.v. dose in the cephalic vein or a s.c. dose between the shoulders. Blood samples were collected predose and 0.25, 1, 2, 6, 12 (monkeys only), 24, 48, 72, 96, 168, 240, and 336 hours postdose into EDTA tubes with 6.3 TIU/ml aprotinin. Multidose PK was also assessed in Wistar Hannover rats and cynomolgus monkeys as part of the Drug Safety Program. Rats (n = 3/sex per dose) weighing 250–300 g received 0.1, 1, 100, and 300 mg/kg i.v. doses in the tail vein. Monkeys (n = 3/sex per dose) weighing 3 to 4 kg received 5, 20, 100, and 300 mg/kg i.v. doses in the cephalic vein. Blood samples were collected predose and 0.25, 2, 6, 24, 48, and 72 hours postdose into EDTA tubes with 6.3 TIU/ml aprotinin. Single-dose PK of total FGF21 and total IgG immunoreactivity of PF-05231023 were assessed in a separate study using Sprague-Dawley rats and cynomolgus monkeys. Male rats (n = 2) weighing 200–225 g received a single 3 mg/kg i.v. dose in the jugular vein. Male monkeys (n = 2) weighing 2.4–3.1 kg received a single 3 mg/kg i.v. dose in the cephalic vein. Blood samples were collected 0.08, 0.5, 1, 3, 5, 7, 24, 48, 72, 96, 120, 144, 192, 240, 312, and 336 hours postdose for rats and at 0.08, 0.5, 1, 4, 6, 12, 24, 36, 48, 72, 96, 120, 144, 168, 192, 240, 288, 336, and 504 hours postdose for monkeys. All PK samples were stored at −80°C until analysis. Rat PK parameters for total IgG were estimated using population modeling of composite steady-state concentrations upon repeat dose administration. Blood samples were collected 0.25, 2, 6, 24, 48, 72, 672, and 1344 hours after the last dose.

FcRn Affinity. pH 6.0 FcRn binding affinities were determined by surface plasmon resonance using previously described methods (Thorn et al., 2012). Two to four replicate experiments were performed for each molecule on a minimum of two different surfaces. Concentrations of PF-05231023 and the unconjugated IgG scaffold of PF-05231023 were varied from 0.1 to at least 5 times the steady-state K_D and were sequentially passed over FcRn.

Serum Stability. In vitro serum stability was assessed using freshly collected Wistar Hannover rat, cynomolgus monkey, or human serum. PF-05231023 was spiked into 1 ml serum on ice, providing an initial concentration of 2 or 20 μg/ml, and was incubated 37°C for 24 hours in a humidified 95%/5% O_2/CO_2 incubator. Sixty microliters of sample was removed at 0, 1, 2, 4, 6, and 24 hours, added to 1.5 μl of 26 TIU/ml aprotinin, flash frozen on dry ice, and stored at −80°C until analysis. N-terminal and C-terminal FGF21 immunoreactivity was measured as described above. Experiments were performed in duplicate.

Human PK Predictions. PK data from rats and monkeys were used to predict CL and PK profiles for N-terminal and C-terminal FGF21 immunoreactivity in humans. CL was prospectively predicted using rat and monkey single-species allometric scaling with a fixed allometric exponent of 0.80. The validity of this exponent was assessed retrospectively by determining the three-species allometric relation in rats, monkeys, and humans by linearizing body weight and CL data on a log-log scale. The mean rat, monkey, and human body weights were 0.25 kg, 3.5 kg, and 87 kg, respectively. Elementary Dedrick analysis was used to scale rat and monkey concentration-time profiles to human concentration-time profiles using an allometric exponent of 1.0 for volume of distribution and 0.80 for CL (Deng et al., 2011). Scaled preclinical data were compared with observed clinical data after a single 200 mg i.v. dose of PF-05231023 (J. Dong et al., submitted manuscript).

PBPK Modeling and Simulations. Standard mAb PBPK models were adapted to simulate the plasma concentration-time profiles for intact CT of FGF21 in rats, monkeys, and humans (Baxter et al., 1995; Garg and Balthasar, 2007; Shah and Betts, 2012). Lymph flows and reflection coefficients were fitted to the mean α- and β-phase half-lives observed for human mAbs displaying linear PK in each species, as well as to published extravascular distribution coefficients (Shah and Betts, 2013). Vascular reflection coefficients for sinusoidal and nonsinusoidal tissues were set to 0.5 and 0.9, respectively. Lymphatic reflection coefficients were set to 0.1. Lymph flows were set to 1300-fold (rats), 1500-fold (monkeys), and 2000-fold (humans) slower than plasma flows in nonpulmonary tissues, and 5000-fold (rats) and 10,000-fold (monkeys and humans) slower than plasma flow in pulmonary tissues (Supplemental Fig. 1; Supplemental Table 1). Rate constants for returning mAbs from lymph to vasculature were set to 0.05 h^{-1}, 0.065 h^{-1}, and 0.014 h^{-1} for rats, monkeys, and humans, respectively. In vitro serum degradation rates for CT of FGF21 were applied to vascular compartments and scaled as necessary to improve model fits. An additional CL term was applied to extravascular compartments to account for the presystemic metabolism of PF-05231023 in

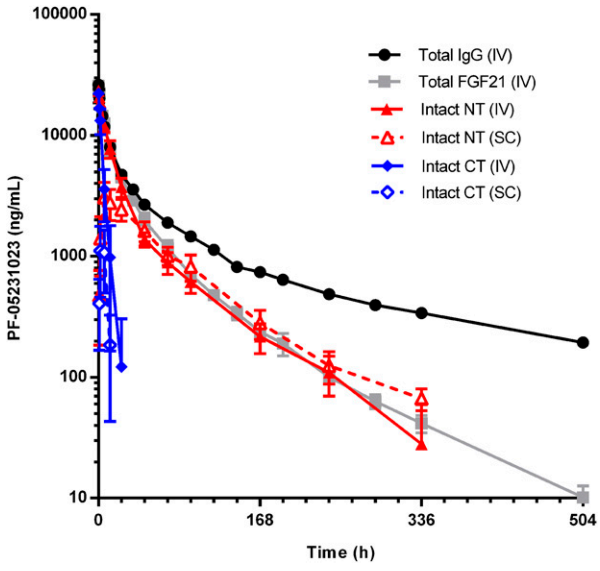

Fig. 2. Mean plasma concentration-time profiles for PF-05231023 in monkeys after a single 1 mg/kg i.v. or s.c. dose. Data for total IgG and total FGF21 were dose normalized to 1 mg/kg.

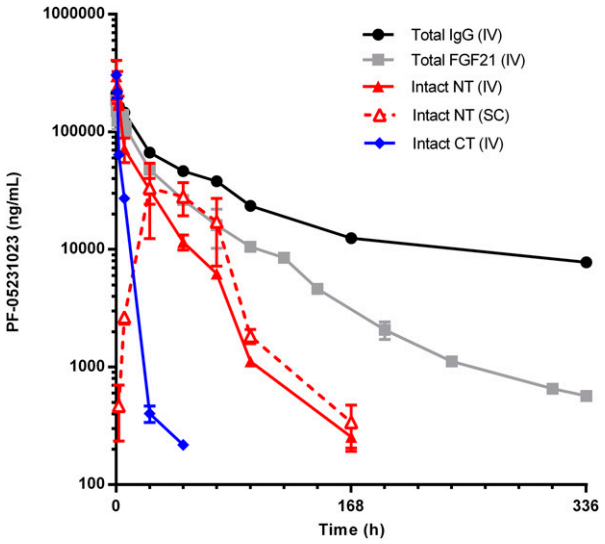

Fig. 3. Mean plasma concentration-time profiles for PF-05231023 in rats after a single 10 mg/kg i.v. or s.c. dose. Data for total FGF21 and total IgG were dose normalized to 10 mg/kg. The PK profile of total IgG was estimated using population modeling of composite steady-state concentrations upon repeat dose administration. ADAs (1%–10% incidence) did not appear to affect the PK of total IgG in rats.

interstitial fluid spaces after s.c. administration. The presystemic extraction ratio in rats and monkeys was estimated by dividing s.c. bioavailability of CT by s.c. bioavailability of NT (representing the minimum extent absorption for intact CT of FGF21). In the rat model, bioavailability of CT was estimated to be approximately 1%, which was the maximum theoretical bioavailability based on the lower limit of quantification of the assay. Human extravascular extraction ratios were set equal to monkey extravascular extraction ratios without further scaling.

Results

Monoclonal detection antibodies, displaying high specificity for the first two N-terminal amino acids (Pro2Ile3) and the last two C-terminal amino acids (Ala180Ser181) of FGF21, were used to determine the PK of PF-05231023. These epitopes overlapped residues required for high-affinity binding and functional activity and are henceforth denoted as intact NT and intact CT of FGF21. Additional assays were designed to measure the mid-region of the FGF21 and IgG scaffold and will henceforth be denoted as total FGF21 and total IgG, respectively. The single-dose PK for PF-05231023 in rats and monkeys is summarized in Tables 1 and 2. Plasma concentration-time profiles for intact NT and CT of FGF21 (Figs. 2 and 3) displayed biphasic kinetics with 25%–57% and 72%–95% of the total area under the curve present under the α-phase, respectively. The mean CL of intact NT and CT of FGF21 ranged from 2.6 to 3.6 ml/h per kg and 11.7 to 12.1 ml/h per kg, respectively. The mean elimination half-life ($t_{1/2}$) for intact NT and CT of FGF21 ranged from 23 to 60 hours and from 3 to 6 hours, respectively. The steady-state volumes of distribution (V_{ss}) for intact NT and CT of FGF21 were 70–100 ml/kg and 38 ml/kg, respectively. As part of Good Laboratory Practice toxicology and safety pharmacology assessments, dose-proportional increases in C_{max} and the area under the curve were observed over the entire dose range examined for intact NT and CT of FGF21 in rats from 0.1 to 300 mg/kg and monkeys from 5 to 300 mg/kg (Table 3).

Mean CL, V_{ss}, and $t_{1/2}$ of total IgG after i.v. administration of PF-05231023 were within 4-fold of the expected range for human mAbs (Giragossian et al., 2013), whereas the intrinsic PK properties of the unmodified IgG scaffold (i.e., without conjugation to the synthetic linker) were within the expected range for human mAbs. Total FGF21 displayed PK parameters intermediate between intact NT of FGF21 and total IgG, compatible with proteolytic degradation occurring in NT of FGF21. The increased CL of total IgG was consistent with reduced affinity of this molecule for FcRn (Table 4). Covalently linking FGF21 to hIgG$_{1\kappa}$ reduced the affinity of PF-05231023 for mouse, monkey, and human FcRn 5-fold, 20-fold, and 30-fold, respectively, compared with the unmodified scaffold.

The single-dose s.c. PK for PF-05231023 is summarized in Figs. 2 and 3; and Table 2. The mean bioavailability of intact NT and CT of FGF21 ranged from 58% to 69% and <1% to 10%, respectively. The T_{max} for intact NT and CT of FGF21 was observed between 6 and 30 hours and at approximately 6 hours, respectively. Half-lives for intact NT of FGF21 were 20.7 and 56.8 hours in rats and monkeys, respectively. The $t_{1/2}$ of intact CT could not be estimated due to insufficient data points with detectable exposure.

To investigate the CL mechanism for PF-05231023, in vitro serum stability of PF-05231023 was assessed in rat, monkey, and human serum (Fig. 4). The percentage of intact NT remaining after 24 hours was greater than 70%. Log-linear half-lives for intact CT in rat, monkey, and human serum were estimated to be 13 hours, 3.5 hours, and 12 hours, respectively, and they were concentration independent from 2 to 20 μg/ml PF-05231023. In vitro serum stability qualitatively reflected the differential in vivo stabilities of intact NT and CT of FGF21 and quantitatively captured in vivo stability differences for intact CT. Directly scaling in vitro serum degradation rates by multiplying the degradation rate by plasma volume accounted for

TABLE 3

Mean dose-normalized C_{max} and AUC_{0-last} after an i.v. dose of PF-05231023 in rats and monkeys

Dose (mg/kg)	n	Total IgG		Intact NT		Intact CT	
		C_{max}/Dose	AUC_{0-72h}/Dose	C_{max}/Dose	AUC_{0-72h}/Dose	C_{max}/Dose	AUC_{0-72h}/Dose
		$\mu g/ml$	$\mu g \cdot h/ml$	$\mu g/ml$	$\mu g \cdot h/ml$	$\mu g/ml$	$\mu g \cdot h/ml$
Rats							
0.1	3	–	–	32.5	424	32.4	147
1	5	–	–	27.9	436	27.3	121
100	6	–	–	25.7	348	26.9	116
300	6	–	–	26.4	383	25.9	138
Monkeys							
5	6	23.4	406	25.2	428	25.0	84.2
20	6	24.4	396	28.8	372	25.0	86.0
100	6	25.0	403	24.8	343	24.1	103
300	6	18.8	407	21.9	420	21.2	123

TABLE 4

Mouse, monkey, and human pH 6.0 FcRn binding affinities for PF-05231023 and the unconjugated $IgG_{1\kappa}$ scaffold of PF-05231023.

Data represent means ± S.D. from two to four experiments.

Species	K_D	
	$IgG_{1\kappa}$	PF-05231023
	nM	
Mouse	2.5 ± 0.9	13 ± 3
Monkey	92 ± 18	1600 ± 200
Human	75 ± 17	2528 ± 11

20%, 70%, and 40% of in vivo CL for intact CT of FGF21 in rats, monkeys, and humans, respectively.

Human CL of PF-05231023 was predicted by simple allometry (Table 5). Using a fixed allometric exponent of 0.80, rat and monkey single-species scaling produced human CL predictions within 1.7-fold of mean values observed in humans. Rat and monkey two-species allometric scaling resulted in human CL predictions within 2.2-fold of mean values observed in humans. Observed three-species allometric exponents for intact NT and CT in rats, monkeys, and humans were retrospectively determined to be 0.75 and 0.82, respectively (Fig. 5).

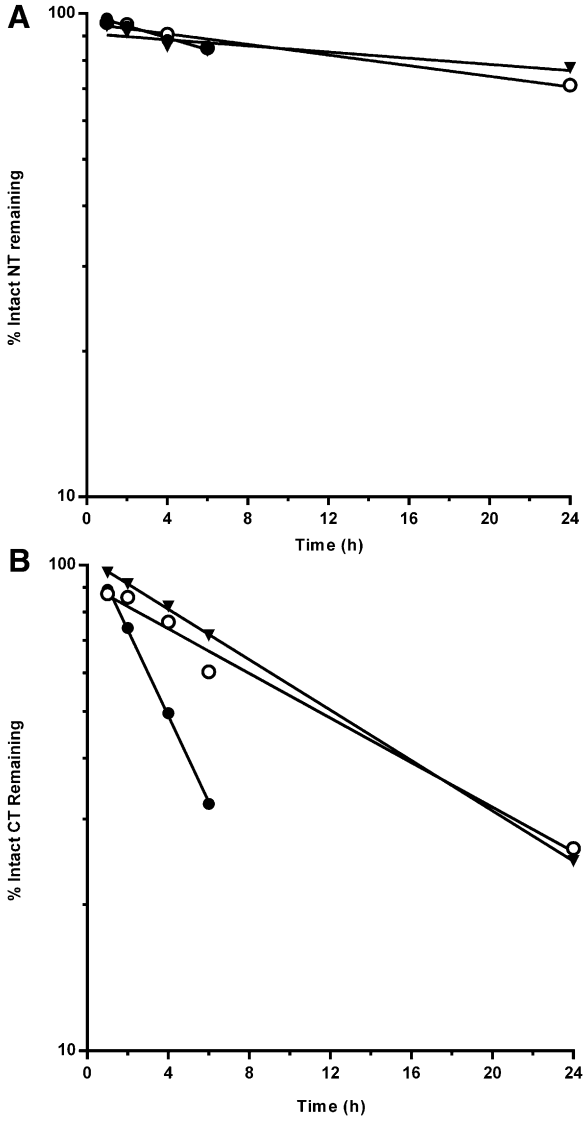

Fig. 4. In vitro stability of PF-05231023 in serum of rats (open circles), monkeys (closed circles), and humans (triangles). (A) Intact NT of FGF21. (B) Intact CT of FGF21. Correlation coefficients for the intact CT of FGF21 were greater than 0.98. Symbols represent the mean of two replicates.

Human plasma concentration-time profiles for intact NT and CT of FGF21 were predicted using elementary Dedrick scaling of rat and monkey plasma concentrations (Fig. 6). Predicted plasma concentrations for intact NT and CT of FGF21, based on Dedrick scaling of monkey PK data, were within 3-fold of observed single-dose human PK data (J. Dong et al., submitted manuscript). Predicted half-lives for intact CT and NT of FGF21 were 8.2 and 103 hours, respectively, and compared favorably with observed human half-lives of 7.3 ± 1.7 and 97 ± 8 hours, respectively. Dedrick scaling of rat PK data resulted in less satisfactory predictions.

In vitro serum degradation rates, estimated in vivo extravascular extraction rates derived from the differential s.c. bioavailability of the intact termini of FGF21, and intrinsic catabolic stability of total IgG were also incorporated into species-specific PBPK models to assess whether these models could improve human PK predictions for intact CT of FGF21 (Fig. 7). Similar to Dedrick scaling, rat PBPK models provided poor fits to observed PK data except when the serum degradation rate was approximately 3-fold faster than the observed rate. By contrast, the monkey PBPK model provided excellent fits to observed data after applying a modest scaling factor (1.25×). Sensitivity analyses indicated the serum degradation rate was critical for capturing the monkey plasma concentration-time profile up to 6 hours postdose, whereas the in vivo extravascular extraction rate was critical for capturing data beyond 6 hours postdose. For the purpose of evaluating prospective human predictions, a 1.25× scaling factor was applied to the human serum degradation rate. Since the rat extravascular extraction rate was poorly defined, monkey extravascular extraction rates were applied to the human PBPK model without further scaling.

The human PBPK model displayed improved fits for intact CT of FGF21 compared with Dedrick scaling. Predicted human plasma concentrations were on average 1.3-fold higher than mean observed concentrations between 0.5 and 73 hours postdose. Similar to the monkey PBPK model, sensitivity analyses indicated that the serum degradation rate was critical for capturing the observed human plasma concentration-time profile up to 25 hours postdose, whereas the in vivo extravascular extraction rate was critical for capturing data beyond 25 hours postdose. Increasing the interstitial fluid extraction ratio from 0.825 to 0.98 adequately captured data beyond 73 hours postdose. Extravascular extraction accounted for 6%, 2%, and 4% of total CL for the intact CT of FGF21 in rats, monkeys, and humans, respectively. Because of the relatively short half-life of the intact CT of FGF21, CL of total IgG contributed minimally to the overall simulation results, comprising an estimated 7%, 5%, and 10% of total CL for the intact CT of FGF21 in rats, monkeys, and humans, respectively. The absence of appreciable degradation of intact NT of FGF21, over the viable quantitative time range for FGF21-related serum proteases, precluded a similar analysis for NT of FGF21.

Discussion

Immunoassays with high specificity for NT and CT of FGF21 were developed to measure PK of PF-05231023 and its major metabolites. Plasma CL of total FGF21, intact NT, and intact CT in monkeys was 90-fold, 80-fold, and 18-fold slower than native rFGF21 and 1.6-fold,

TABLE 5

Comparison of predicted and observed mean human CL values for PF-05231023

Data represent the mean or mean ± S.D. Monkey and rat CL values for the intact NT and CT of FGF21 were scaled to human CL values using a fixed allometric exponent of 0.80.

Scaling Method	Human CL	
	NT	CT
	l/h	
Rat single-species	0.097	0.32
Monkey single-species	0.12	0.55
Two-species	0.15	1.1
Observed human	0.070 ± 0.019	0.49 ± 0.26

1.8-fold, and 8-fold faster than the $IgG_{1\kappa}$ scaffold of PF-05231023. CL of the conjugated $IgG_{1\kappa}$ scaffold was approximately 4-fold faster than the native unconjugated mAb (data not shown) and approached CL values expected for complete ablation of FcRn binding (Waldmann and Terry, 1990; Hakimi et al., 1991; Hutzell et al., 1991; Saravolatz et al., 1994; He et al., 1998; Garg and Balthasar, 2007). Increased CL of total IgG may be associated with reduced affinity of PF-05231023 for FcRn; however, this may not be the only factor, because CL of total IgG was predicted to be slower in rodents compared with primates based on species differences in FcRn affinity. Although it is possible that rat FcRn behaves differently than mouse FcRn, previous studies have shown only minor differences in hIgG affinity for rat and mouse FcRn, as would be expected based on conserved FcRn binding-site homology and glycosylation patterns (Neuber et al., 2014).

Other potential sources for accelerated CL of total IgG include specific interactions with FGFRs, anti-drug antibodies (ADAs), and nonspecific interactions with endogenous molecules. The PK of intact NT, intact CT, and total IgG was linear in rats and monkeys across the entire dose range examined, consistent with absence of appreciable target-mediated disposition. Linear PK for intact NT and CT was also observed in humans across the entire dose range examined from 0.5 to 200 mg (J. Dong et al., submitted manuscript).

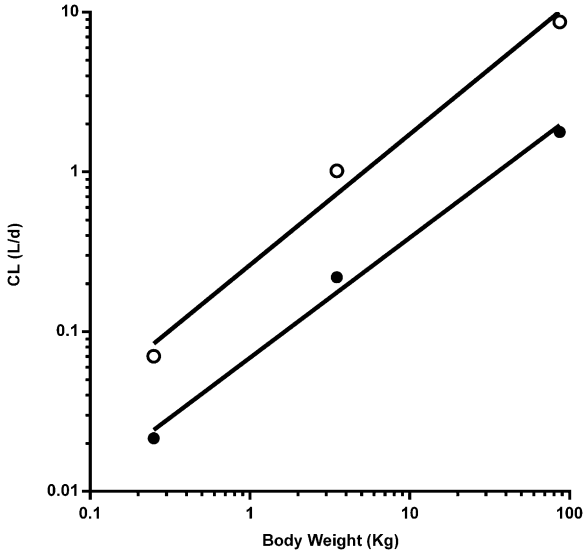

Fig. 5. Allometric relationship for CL of PF-05231023 in rats, monkeys, and humans. Allometric coefficients and exponents were 0.0029 and 0.75, respectively, for intact NT of FGF21 (closed circles) and 0.011 and 0.82, respectively, for intact CT (open circles) of FGF21. Correlation coefficients were greater than 0.98.

ADAs were undetectable in all species after a single dose, and there was no evidence for accelerated CL during the terminal phase that would point to formation of clearing ADAs. The relatively acidic isoelectric point of PF-05231023 (pI = 7.6) and the absence of positively charged clusters in the FGF19-based homology model of FGF21 suggest that nonspecific interactions with negatively charged cell membranes were unlikely to contribute to accelerated CL compared with the unconjugated mAb (pI = 8.5); however, nonspecific interactions with other endogenous molecules cannot be excluded.

Covalently linking rFGF21 to an antibody scaffold shifted the primary CL mechanism of FGF21 from passive renal filtration to proteolytic degradation. This was supported by the fact that CL of intact NT and CT of unconjugated rFGF21 was identical in mice, as well as by the observed correlation between endogenous FGF21 levels and renal function in humans (Stein et al., 2009; Hager et al., 2013). Differential stabilities of NT, CT, and total FGF21 immunoreactivity in PF-05231023 indicated that multiple proteolytic cleavage sites were present throughout the FGF21 sequence. Scaled in vitro serum degradation rates for intact CT of FGF21 in monkeys and humans suggested that the principal CL route of PF-05231023 was degradation by serum proteases in these species, whereas serum proteases accounted for only 20% of CL in rats.

CL of intact CT of FGF21 in PF-05231023 was comparable to CL of intact Fc-FGF21. The rate-limiting cleavage site in rFGF21 in vitro (data not shown) and in vivo was identified in CT between Pro171 and Ser172 (Hager et al., 2013). Stabilization of the Pro171/Ser172 cleavage site in Fc-FGF21 by site-directed mutagenesis decreased CL of Fc-FGF21 5-fold in monkeys. Consistent with results presented for PF-05231023, stabilization of the principal C-terminal cleavage site in Fc-FGF21 shifted metabolism to other sites within FGF21 sequence, because CL of intact Fc-FGF21 was still considerably faster than CL of total Fc. In line with these observations, additional cleavage sites were putatively identified in CT of Fc-FGF21 (Hager et al., 2013).

The moderately increased molecular mass of PF-05231023 (189 kDa versus 150 kDa) did not appear to alter apparent V_{ss} or intercompartmental CL rates compared with therapeutic mAbs. V_{ss} values for intact NT, total FGF21, and total IgG were comparable and 2- to 4-fold higher than plasma volume, whereas V_{ss} for intact CT was comparable to plasma volume. Reduced apparent V_{ss} for intact CT, compared with other drug-related products of PF-05231023, was compatible with proteolysis occurring outside the serum compartment (Richter et al., 2012). Similar findings were observed in humans, in which the mean V_{ss} for intact NT and CT ranged from 74 to 86 ml/kg and 49 to 59 ml/kg, respectively (J. Dong et al., submitted manuscript).

The bioavailability of intact NT was similar in rats and monkeys; however, a greater than 10-fold difference was observed for bioavailability of intact CT. Differential bioavailability of intact NT compared with CT paralleled in vitro and in vivo stabilities of these moieties, and may be indicative of differential susceptibility to injection-site proteases and/or presystemic proteolysis via the lymphatic system. Relatively high bioavailability for intact NT excluded aggregation or nonspecific/specific uptake by macrophages or lymph nodes. Interestingly, species differences in bioavailability for intact CT were not correlated with in vitro serum or in vivo stability, suggesting the existence of an alternate protease with overlapping substrate specificity and/or differential expression of proteases between serum and extravascular tissue spaces. Although the precise mechanisms responsible for reduced bioavailability of intact CT have not been elucidated, injection site

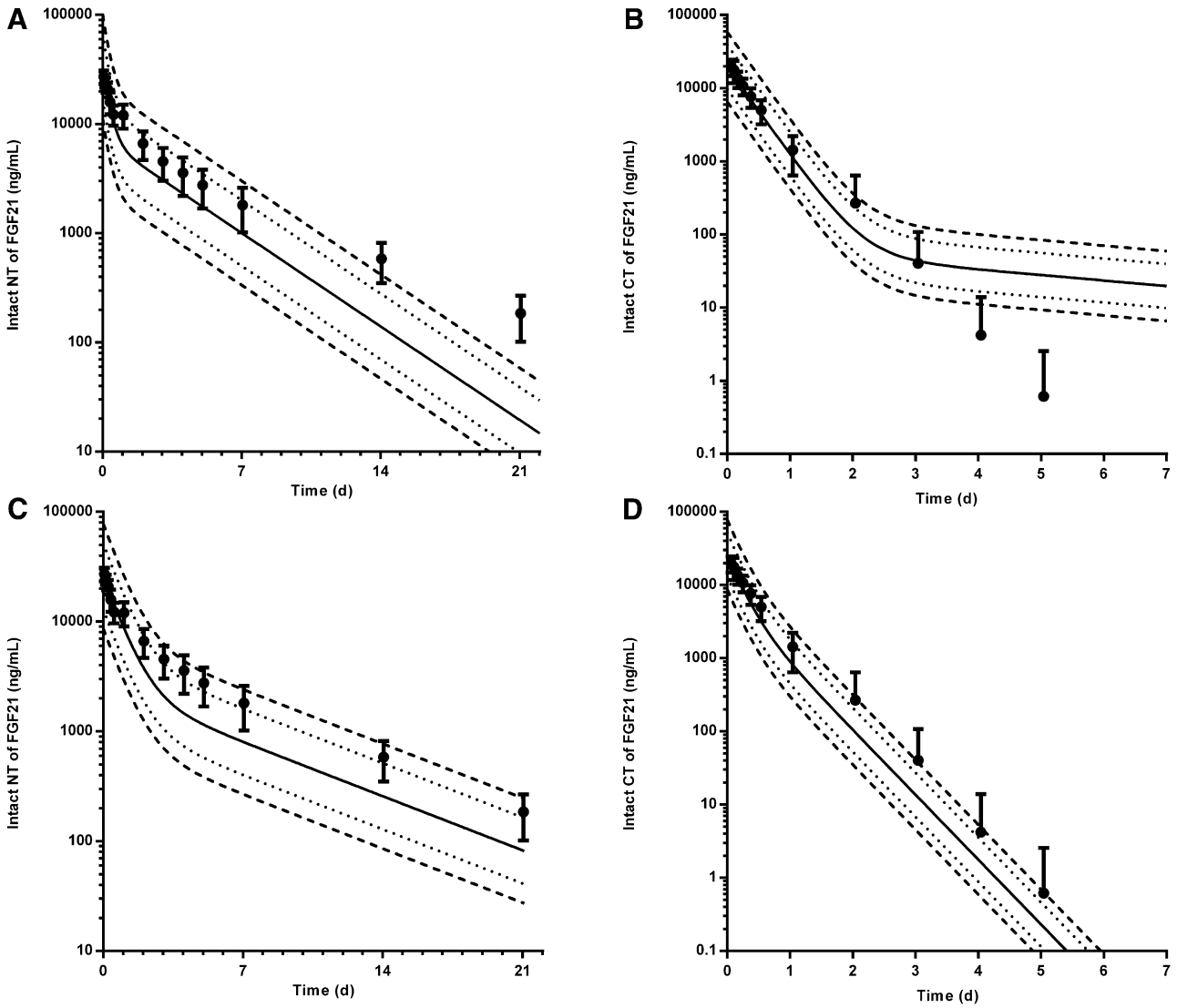

Fig. 6. Predicted human PF-05231023 plasma concentration-time profiles for intact NT and intact CT of FGF21 as determined by elementary Dedrick scaling of rat (A and B) and monkey (C and D) PK data. Volume of distribution and CL were scaled with allometric exponents of 1.0 and 0.80, respectively. Observed human PK data were dose normalized to 1 mg/kg. Dotted and dashed lines denote 2- and 3-fold prediction limits, respectively.

degradation and presystemic lymphatic extraction were previously reported for other therapeutic proteins (Charman et al., 2000; Wang et al., 2012).

Human CL predictions based on rat and monkey single-species scaling using a fixed allometric exponent of 0.80 were within 2-fold of clinically observed values for intact NT and CT of FGF21. A fixed exponent of 0.80 was previously shown to be an appropriate single-species scaling factor for predicting human CL for a wide variety of therapeutic proteins and mAbs (Wang and Prueksaritanont, 2010). Other studies based on an overlapping data set of therapeutic mAbs supported use of a fixed exponent ranging from 0.75 to 0.90 to predict human CL from monkey (Ling et al., 2009; Deng et al., 2011; Dong et al., 2011; Oitate et al., 2011, 2012). The range of exponents reported for mAbs is not surprising, given the relative insensitivity of this parameter toward single-species scaling between monkeys and humans (e.g., an exponent between 0.67 and 0.90 results in an approximately 2-fold change in predicted human CL). Retrospective analysis of the three-species allometric relation for intact NT and CT in rats, monkeys, and humans provided further support for selection of a fixed exponent of 0.80. Although both rats and monkeys provided fairly good human CL predictions, elementary Dedrick scaling of monkey plasma concentrations was qualitatively and quantitatively superior to rodent scaling, which is in agreement with previous reports (Deng et al., 2011).

In vitro serum stability generally tends to underestimate in vivo CL for biologics (Pauwels et al., 1985; Deacon et al., 1995; Hartmann et al., 2000). The poor in vitro–in vivo translation likely results from several factors such as the loss of intrinsic activity upon harvesting serum, membrane-associated intravascular/extravascular proteases, soluble interstitial fluid proteases, and other mechanisms associated with CL of complex biologics. Species differences in serum degradation rates and extravascular extraction ratios indicated that in vitro serum stability data alone were unlikely to provide robust human CL predictions for PF-0523102 and other FGF21 analogs.

Integrating in vitro and in vivo measures into a PBPK modeling framework provided a flexible platform for interrogating relative contributions of various CL mechanisms and their subsequent

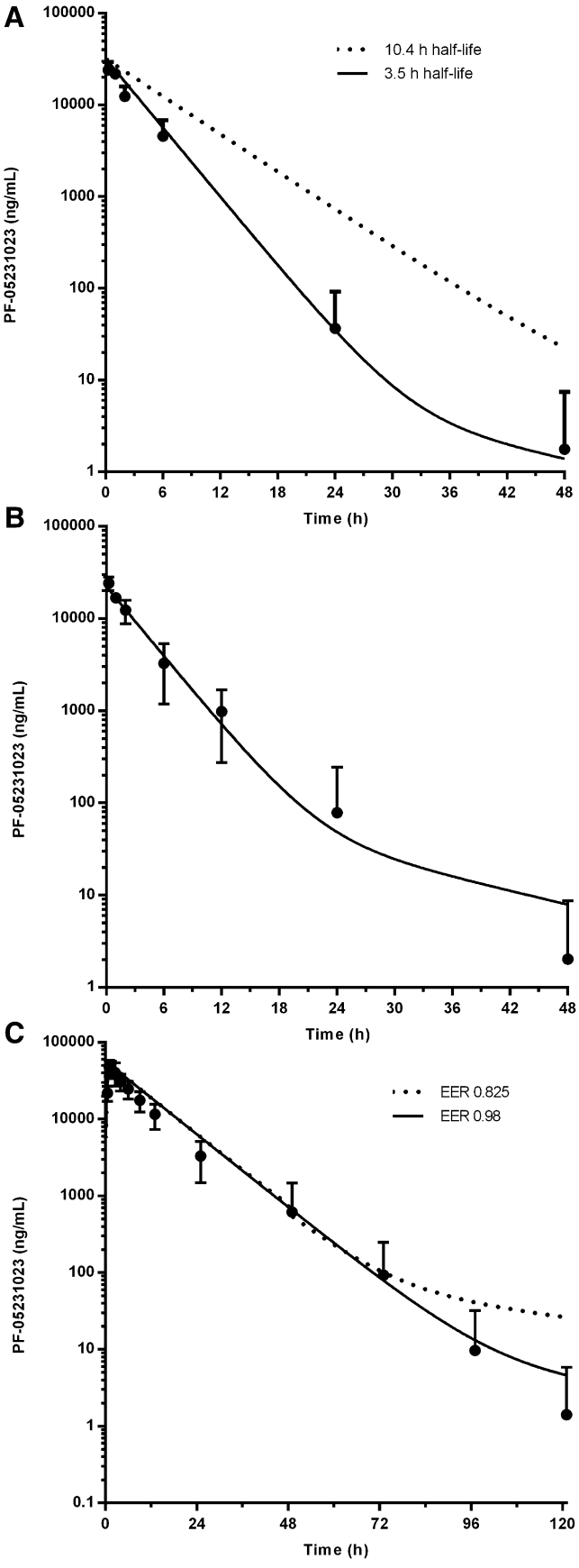

Fig. 7. PBPK model predicted and observed PF-05231023 plasma concentrations for intact CT of FGF21 in rats (A), monkeys (B), and humans (C). Rat and monkey data were dose normalized to 1 mg/kg, and human data were dose normalized to 2.3 mg/kg. Serum degradation half-lives were set to 10.4 or 3.5 hours for rats, 2.3 hours for monkeys, and 9.6 hours for humans. The extravascular extraction ratio (EER) was set to 0.99 for rats, 0.825 for monkeys, and 0.825 or 0.98 for humans.

influence on plasma concentration-time profiles. Rate-limiting extravasation, as inferred by the α-phase half-life of mAbs, placed significant constraints on CL contributions mediated by interstitial fluid proteases after i.v. administration. The inability of the rat PBPK model to capture the shorter than expected α-phase half-life of intact CT implied species differences in physiology and/or additional uncharacterized CL mechanisms. Although both rat and monkey single-species scaling did an adequate job of predicting human CL, the apparent disconnect in CL mechanisms between rats and monkeys would prospectively point to the monkey as the preferred species for human predictions, based purely on phylogeny. The observed human in vitro serum degradation rate for intact CT was approximately 2-fold slower than predicted by allometrically scaling the monkey in vitro degradation rate. This coupled with the fact that serum degradation represents the principal CL mechanism of intact CT in monkeys and humans explains why monkey single-species allometric scaling of in vivo CL does a fairly good job of predicting human CL despite apparent differences in serum stability. In alignment with these findings, human PBPK predictions for intact CT were more accurate compared with monkey Dedrick scaling, which underpredicted human plasma concentrations by 2- to 3-fold during the terminal elimination phase.

In conclusion, immunoassays with high specificity for intact NT and CT of FGF21 demonstrated that PF-05231023 was subjected to rapid proteolysis within the CT, the same region of the molecule critical for maintaining in vitro potency through its interactions with β-klotho. In vitro serum stability studies suggested that the principal CL route of PF-05231023 in monkeys and humans was degradation by an as yet unidentified serum protease(s). Incorporating in vitro and in vivo measures into PBPK models provided superior human PK predictions compared with elementary Dedrick scaling. This type of mechanism-based PBPK modeling may find broad applicability for predicting human PK of complex biologics, including fusion proteins and synthetically conjugated proteins.

Acknowledgments

The authors thank their Comparative Medicine colleagues at Pfizer for performing routine animal husbandry, Frank Geoly and Kathryn Gropp for conducting the multiple-dose toxicology studies, Legacy Pfizer CovX colleagues for conducting animal studies and providing bioanalytical support to enable PK assessment for total FGF21 and total IgG, and Jeffery Chabot and Jennifer Dong for critically reading the manuscript and providing helpful comments.

Authorship Contributions

Participated in research design: Giragossian, Vage, Pelletier, Piché-Nicholas, Rajadhyaksha, Liras, Logan, Calle, Weng.

Conducted experiments: Giragossian, Li, Pelletier, Piché-Nicholas, Logan.

Contributed new reagents or analytic tools: Pelletier, Rajadhyaksha, Liras, Logan.

Performed data analysis: Giragossian, Vage, Li, Pelletier, Piché-Nicholas, Calle, Weng.

Wrote or contributed to the writing of the manuscript: Giragossian, Piché-Nicholas, Calle, Weng.

References

Adams AC, Halstead CA, Hansen BC, Irizarry AR, Martin JA, Myers SR, Reynolds VL, Smith HW, Wroblewski VJ, and Kharitonenkov A (2013) LY2405319, an engineered FGF21 variant, improves the metabolic status of diabetic monkeys. *PLoS ONE* **8**:e65763.

Baxter LT, Zhu H, Mackensen DG, Butler WF, and Jain RK (1995) Biodistribution of monoclonal antibodies: scale-up from mouse to human using a physiologically based pharmacokinetic model. *Cancer Res* **55**:4611–4622.

Belouski EJ, Ellison MM, Hamburger AE, Hecht RI, Li YS, Michaels ML, Sun J, and Xu J (2010) inventors, Amgen Inc., assignee. Fgf21 mutants and uses thereof. U.S. patent US20100285131 A1. 2010 Nov 11.

Charman SA, Segrave AM, Edwards GA, and Porter CJ (2000) Systemic availability and lymphatic transport of human growth hormone administered by subcutaneous injection. *J Pharm Sci* **89**:168–177.

Deacon CF, Johnsen AH, and Holst JJ (1995) Degradation of glucagon-like peptide-1 by human plasma in vitro yields an N-terminally truncated peptide that is a major endogenous metabolite in vivo. *J Clin Endocrinol Metab* **80**:952–957.

Deng R, Iyer S, Theil FP, Mortensen DL, Fielder PJ, and Prabhu S (2011) Projecting human pharmacokinetics of therapeutic antibodies from nonclinical data: what have we learned? *MAbs* **3**:61–66.

Dong JQ, Salinger DH, Endres CJ, Gibbs JP, Hsu CP, Stouch BJ, Hurh E, and Gibbs MA (2011) Quantitative prediction of human pharmacokinetics for monoclonal antibodies: retrospective analysis of monkey as a single species for first-in-human prediction. *Clin Pharmacokinet* **50**: 131–142.

Gaich G, Chien JY, Fu H, Glass LC, Deeg MA, Holland WL, Kharitonenkov A, Bumol T, Schilske HK, and Moller DE (2013) The effects of LY2405319, an FGF21 analog, in obese human subjects with type 2 diabetes. *Cell Metab* **18**:333–340.

Garg A and Balthasar JP (2007) Physiologically-based pharmacokinetic (PBPK) model to predict IgG tissue kinetics in wild-type and FcRn-knockout mice. *J Pharmacokinet Pharmacodyn* **34**: 687–709.

Gimeno RE and Moller DE (2014) FGF21-based pharmacotherapy—potential utility for metabolic disorders. *Trends Endocrinol Metab* **25**:303–311.

Giragossian C, Clark T, Piché-Nicholas N, and Bowman CJ (2013) Neonatal Fc receptor and its role in the absorption, distribution, metabolism and excretion of immunoglobulin G-based biotherapeutics. *Curr Drug Metab* **14**:764–790.

Hager T, Spahr C, Xu J, Salimi-Moosavi H, and Hall M (2013) Differential enzyme-linked immunosorbent assay and ligand-binding mass spectrometry for analysis of biotransformation of protein therapeutics: application to various FGF21 modalities. *Anal Chem* **85**:2731–2738.

Hakimi J, Chizzonite R, Luke DR, Familletti PC, Bailon P, Kondas JA, Pilson RS, Lin P, Weber DV, and Spence C, et al. (1991) Reduced immunogenicity and improved pharmacokinetics of humanized anti-Tac in cynomolgus monkeys. *J Immunol* **147**:1352–1359.

Hartmann B, Harr MB, Jeppesen PB, Wojdemann M, Deacon CF, Mortensen PB, and Holst JJ (2000) In vivo and in vitro degradation of glucagon-like peptide-2 in humans. *J Clin Endocrinol Metab* **85**:2884–2888.

He XY, Xu Z, Melrose J, Mullowney A, Vasquez M, Queen C, Vexler V, Klingbeil C, Co MS, and Berg EL (1998) Humanization and pharmacokinetics of a monoclonal antibody with specificity for both E- and P-selectin. *J Immunol* **160**:1029–1035.

Hecht R, Li YS, Sun J, Belouski E, Hall M, Hager T, Yie J, Wang W, Winters D, and Smith S, et al. (2012) Rationale-Based Engineering of a Potent Long-Acting FGF21 Analog for the Treatment of Type 2 Diabetes. *PLoS ONE* **7**:e49345.

Huang J, Ishino T, Chen G, Rolzin P, Osothprarop TF, Retting K, Li L, Jin P, Matin MJ, and Huyghe B, et al. (2013) Development of a novel long-acting antidiabetic FGF21 mimetic by targeted conjugation to a scaffold antibody. *J Pharmacol Exp Ther* **346**:270–280.

Hutzell P, Kashmiri S, Colcher D, Primus FJ, Hand PH, Roselli M, Finch M, Yarranton G, Bodmer M, and Whittle N, et al. (1991) Generation and characterization of a recombinant/chimeric B72.3 (human gamma 1). *Cancer Res* **51**:181–189.

Kharitonenkov A, Beals JM, Micanovic R, Strifler BA, Rathnachalam R, Wroblewski VJ, Li S, Koester A, Ford AM, and Coskun T, et al. (2013) Rational design of a fibroblast growth factor 21-based clinical candidate, LY2405319. *PLoS ONE* **8**:e58575.

Kharitonenkov A, Wroblewski VJ, Koester A, Chen YF, Clutinger CK, Tigno XT, Hansen BC, Shanafelt AB, and Etgen GJ (2007) The metabolic state of diabetic monkeys is regulated by fibroblast growth factor-21. *Endocrinology* **148**:774–781.

Ling J, Zhou H, Jiao Q, and Davis HM (2009) Interspecies scaling of therapeutic monoclonal antibodies: initial look. *J Clin Pharmacol* **49**:1382–1402.

Micanovic R, Raches DW, Dunbar JD, Driver DA, Bina HA, Dickinson CD, and Kharitonenkov A (2009) Different roles of N- and C- termini in the functional activity of FGF21. *J Cell Physiol* **219**:227–234.

Mu J, Pinkstaff J, Li Z, Skidmore L, Li N, Myler H, Dallas-Yang Q, Putnam AM, Yao J, and Bussell S, et al. (2012) FGF21 analogs of sustained action enabled by orthogonal biosynthesis demonstrate enhanced antidiabetic pharmacology in rodents. *Diabetes* **61**:505–512.

Neuber T, Frese K, Jaehrling J, Jäger S, Daubert D, Felderer K, Linnemann M, Höhne A, Kaden S, and Kölln J, et al. (2014) Characterization and screening of IgG binding to the neonatal Fc receptor. *MAbs* **6**:928–942.

Oitate M, Masubuchi N, Ito T, Yabe Y, Karibe T, Aoki T, Murayama N, Kurihara A, Okudaira N, and Izumi T (2011) Prediction of human pharmacokinetics of therapeutic monoclonal antibodies from simple allometry of monkey data. *Drug Metab Pharmacokinet* **26**:423–430.

Oitate M, Nakayama S, Ito T, Kurihara A, Okudaira N, and Izumi T (2012) Prediction of human plasma concentration-time profiles of monoclonal antibodies from monkey data by a species-invariant time method. *Drug Metab Pharmacokinet* **27**:354–359.

Pauwels S, Dockray GJ, Walker R, and Marcus S (1985) Metabolism of heptadecapeptide gastrin in humans studied by region-specific antisera. *J Clin Invest* **75**:2006–2013.

Reitman ML (2013) FGF21 mimetic shows therapeutic promise. *Cell Metab* **18**:307–309.

Richter WF, Bhansali SG, and Morris ME (2012) Mechanistic determinants of biotherapeutics absorption following SC administration. *AAPS J* **14**:559–570.

Saravolatz LD, Wherry JC, Spooner C, Markowitz N, Allred R, Remick D, Fournel M, and Pennington JE (1994) Clinical safety, tolerability, and pharmacokinetics of murine monoclonal antibody to human tumor necrosis factor-alpha. *J Infect Dis* **169**:214–217.

Shah DK and Betts AM (2012) Towards a platform PBPK model to characterize the plasma and tissue disposition of monoclonal antibodies in preclinical species and human. *J Pharmacokinet Pharmacodyn* **39**:67–86.

Shah DK and Betts AM (2013) Antibody biodistribution coefficients: inferring tissue concentrations of monoclonal antibodies based on the plasma concentrations in several preclinical species and human. *MAbs* **5**:297–305.

Smith R, Duguay A, Bakker A, Li P, Weiszmann J, Thomas MR, Alba BM, Wu X, Gupte J, and Yang L, et al. (2013) FGF21 can be mimicked in vitro and in vivo by a novel anti-FGFR1c/β-Klotho bispecific protein. *PLoS ONE* **8**:e61432.

Stein S, Bachmann A, Lössner U, Kratzsch J, Blüher M, Stumvoll M, and Fasshauer M (2009) Serum levels of the adipokine FGF21 depend on renal function. *Diabetes Care* **32**:126–128.

Thorn M, Piche-Nicholas N, Stedman D, Davenport SW, Zhang N, Collinge M, and Bowman CJ (2012) Embryo-fetal transfer of bevacizumab (Avastin) in the rat over the course of gestation and the impact of neonatal Fc receptor (FcRn) binding. *Birth Defects Res B Dev Reprod Toxicol* **95**:363–375.

Waldmann TA and Terry WD (1990) Familial hypercatabolic hypoproteinemia. A disorder of endogenous catabolism of albumin and immunoglobulin. *J Clin Invest* **86**:2093–2098.

Wang W, Chen N, Shen X, Cunningham P, Fauty S, Michel K, Wang B, Hong X, Adreani C, and Nunes CN, et al. (2012) Lymphatic transport and catabolism of therapeutic proteins after subcutaneous administration to rats and dogs. *Drug Metab Dispos* **40**:952–962.

Wang W and Prueksaritanont T (2010) Prediction of human clearance of therapeutic proteins: simple allometric scaling method revisited. *Biopharm Drug Dispos* **31**:253–263.

Yie J, Hecht R, Patel J, Stevens J, Wang W, Hawkins N, Steavenson S, Smith S, Winters D, and Fisher S, et al. (2009) FGF21 N- and C-termini play different roles in receptor interaction and activation. *FEBS Lett* **583**:19–24.

Address correspondence to: Yan Weng, Pharmacokinetics, Dynamics, and Metabolism, Pfizer Worldwide Research and Development, 610 Main St., Cambridge, MA 02139. E-mail: yan.weng2@pfizer.com